From eqn. 3, it is clear that the log-gains of all channels are linear functions of the reservoir r only. We can also rewrite eqn. 3 in a more familiar form as $G_k(t) = \rho L\Gamma_k(\sigma_k^T x(t) - \sigma_k^a)$, where $x(t) \triangleq (1/L)\int_0^L N_2(z, t)dz$ is the mean fraction of excited ions [2].

Multiplying both sides of eqn. 1 by dz and integrating from 0 to L yields

$$\frac{\partial r(t)}{\partial t} = -\frac{r(t)}{\tau} - \sum_{j=0}^{N}(Q_j^{out} - Q_j^{in}) \qquad (4)$$

Using eqn. 3 in eqn. 4, we finally obtain a first-order differential equation describing the dynamic time behaviour of the system's state, i.e. the reservoir $r(t)$:

$$\dot{r}(t) = -\frac{r(t)}{\tau} + \sum_{j=0}^{N} Q_j^{in}\left(1 - e^{B_j r(t) - A_j}\right) \qquad (5)$$

Once the initial condition $r(0) = r_0$ is specified, the solution of eqn. 5 is unique. r_0 can be any number in the allowed range $[0, \rho AL]$. However, if at time $t = 0^-$, i.e. one instant before the start of the observation period, the amplifier is at equilibrium, then r_0 must satisfy eqn. 5 with $\dot{r}(0^-) = 0$:

$$r_0 = \tau \sum_{j=0}^{N} Q_j^{in}(0^-)\left(1 - e^{B_j r_0 - A_j}\right) \qquad (6)$$

which is the well-known Saleh steady state equation [3]. For a starting guess in its numerical solution, the upper bound $\tau\Sigma_{j=0}^{N} Q_j^{in}(0^-)$ can be used.

Note that, since by eqn. 5 the derivative of r exists, r is a continuous function of t, even when the inputs $\{Q_j^{in}\}$ are discontinuous. In exactly the same way as for charge on a capacitor, the reservoir cannot 'jump' instantaneously. Note also that eqn. 5 has a nice physical meaning: the variation of the reservoir (the 'charge' on the amplifier) is given by the total input flux $\Sigma_{j=0}^{N} Q_j^{in}$, minus the output flux $\Sigma_{j=0}^{N} Q_j^{out}$, minus the spontaneous decay from the excited level r/τ.

Hence, by identifying photon fluxes with currents, and the reservoir with the charge on a capacitor, or better yet with the voltage across a capacitor of capacity $C = 1$, we obtain the equivalent electric circuit depicted in Fig. 1*a*. The circuit is composed of N input current sources (the channels) and of a pump channel 0, hidden inside the amplifier. The currents feed the capacitor, whose voltage is the reservoir r. The currents out are voltage-controlled current generators, whose gain is $g_j(r) = e^{G_j(r)}$. The output pump current is shunted to ground and does not exit the amplifier. The RC constant of the capacitive circuit is τ. However, this is an active circuit, and it is clear that the actual time constants involved in the dynamics are essentially independent of τ.

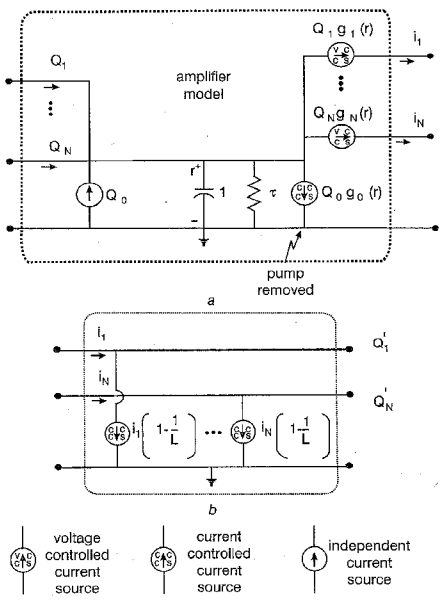

Fig. 1 *Fibre amplifier equivalent circuit and that for optical loss L*

a Fibre amplifier equivalent circuit
b For optical loss L

The circuit model for a subsequent loss L is shown in Fig. 1*b*. It is simply a bank of current-controlled current generators that shunt part of the output photons to ground, effectively wasting them.

Using these building blocks for the amplifier and the loss, any complex network of amplifiers is readily solved by any electric circuit simulator available on the market.

Acknowledgments: This work was supported by the European Community under INCO-DC project No 950959 'DAWRON', and by an NSERC Industrial Chair sponsored by Québec-Téléphone.

21 July 1997
Electronics Letters Online No: 19971273

A. Bononi (*Università di Parma, Dipartimento di Ingegneria dell'Informazione, I-43100 Parma, Italy*)

L.A. Rusch and L. Tancevski (*Université Laval, Département de Génie Électrique et de Génie Informatique, Québec, G1K 7P4, Canada*)

References

1 SUN, Y., LUO, G., ZYSKIND, J.L., SALEH, A.A.M., SRIVASTAVA, A.K., and SULHOFF, J.W.: 'Model for gain dynamics in erbium-doped fibre amplifiers', *Electron. Lett.*, 1996, **32**, pp. 1490–1491

2 GEORGES, T., and DELEVAQUE, E.: 'Analytic modeling of high-gain erbium-doped fibre amplifiers', *Opt. Lett.*, 1992, **17**, pp. 1113–1115

3 SALEH, A.A.M., JOPSON, R.M., EVANKOV, J.D., and ASPELL, J.: 'Modeling of gain in erbium-doped fibre amplifiers', *IEEE Photonics Technol. Lett.*, 1990, **2**, pp. 714–717

Suppression of optical beat interference using synchronised CDMA technique and in-band clipping carrier

B.H. Wang, C.C. Hsiao and W.I. Way

Indexing terms: Code division multiple access, Multi-access systems, Optical communication

The authors propose adding a coherent in-band clipping carrier to a previously demonstrated Walsh-code-based synchronised CDMA (S-CDMA) technique to further suppress the optical beat interference (OBI). Experimental results showed that a negligible system power penalty can be achieved even when the OBI-induced intensity noise was as high as –90.9dB/Hz. In addition, a large system dynamic range of 10dB can be obtained to relax the tight power control requirement on S-CDMA signals.

Introduction: The feasibility of using a Walsh-code-based synchronised CDMA (S-CDMA) technique to achieve multiple access in the presence of optical-beat and co-channel interference was previously demonstrated [1]. While conventional OBI suppression techniques such as out-of-band clipping-tone [2, 3] or over-modulating multiple frequency-division-multiplexed channels [4, 5] could cause in-band nonlinear distortions, the S-CDMA technique can effectively suppress the OBI without incurring the same problem and at the same time enjoy the full bandwidth of an optical fibre system. However, owing to the fact that a broadband CDMA cannot suppress OBI as effectively as narrow-band clipping tones, we found that some residual system penalties remained due to incomplete suppression of the OBI [1]. Therefore, in this Letter, we propose adding an *in-band* clipping carrier to the S-CDMA signal, to further suppress the residual OBI without using additional system bandwidth. By implementing this technique, the power control tolerance of the optical transmitters can be relieved by ~8dB compared to that of the previous case [1].

Experiment: Our experimental setup is shown in Fig. 1. An S-CDMA signal and an in-band clipping carrier were coherently combined and used to modulate a 1.3μm DFB laser (laser A). The S-CDMA signal was generated by spreading a 1.5625Mbit/s, 2^{20}–1

pseudorandom data with a 200Mbit/s Walsh code (using Walsh code generator#1) which had a code length of 128, and was up-converted by a 672MHz RF carrier. Note that the 672MHz carrier served as both the upconverter local oscillator and the in-band clipping carrier. The OBI was generated by using laser B and a delayed self-homodyne interferometer (DSI) setup. Various OBI levels were obtained by adjusting the tunable optical attenuator following the DSI. The modulation indices in both laser A and B were adjusted to be the same. The received signal and the OBI were both down-converted by a perfectly-phase-locked 672MHz carrier and subsequently de-spread by a perfectly-synchronised Walsh code.

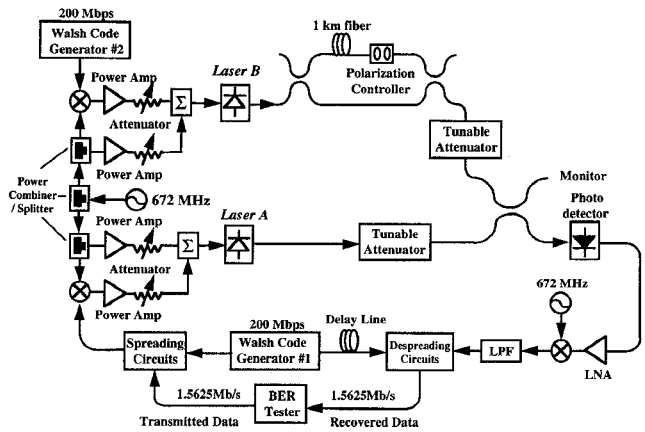

Fig. 1 *Experimental setup*

The minimum received optical power from laser A, P_A, at a photo-detector when the $BER = 10^{-9}$ was measured for four different cases: (i) S-CDMA signal modulation without OBI; (ii) S-CDMA signal and in-band clipping carrier modulation without OBI; (iii) S-CDMA signal modulation with OBI and (iv) S-CDMA signal and in-band clipping carrier modulation with OBI. In the measurement we arbitrarily let the S-CDMA signal and clipping carrier have equal power, i.e. $MI_S = MI_C$ (MI_S and MI_C are the modulation indices of the S-CDMA signal and clipping carrier, respectively). Fig. 2 shows the measured results when the received optical power from DSI, P_B, is –19dBm. We can see that, with OBI present, the minimum P_A can be improved by ~5dB due to the addition of a clipping carrier. However, when comparing cases (i) and (ii), we note that there is a < 2dB system power penalty. This is because the clipping carrier introduced some non-linear distortions into the S-CDMA signal.

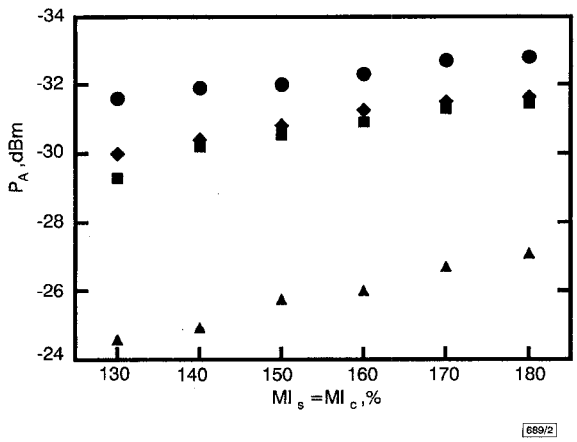

Fig. 2 *Minimum required received power from laser A (P_A) at BER = 10^{-9} against CDMA signal modulation index MI_S and clipping carrier modulation index MI_C*

● S-CDMA only, no OBI
◆ S-CDMA and clipping carrier, no OBI
■ S-CDMA and clipping carrier, with OBI
▲ S-CDMA only, with OBI

Fig. 3 illustrates the RF spectra of OBI before and after the S-CDMA signal and a coherent in-band clipping carrier were applied. The modulation indices of both signals were 180% and P_B = –19dBm. It can be seen that the OBI level was suppressed by at least 10dB and the peak OBI level was suppressed by as much as 37dB.

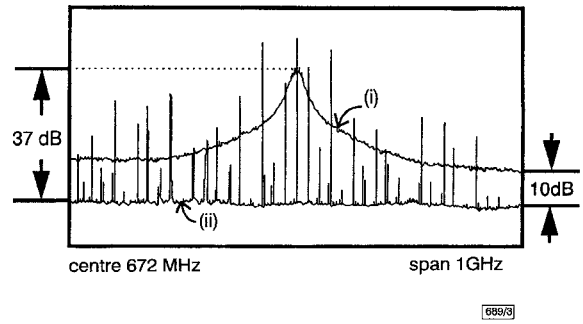

Fig. 3 *Spectra of OBIs before and after S-CDMA and in-band clipping carrier were applied*

Modulation indices of both applied signals were 180%
a Before
b After

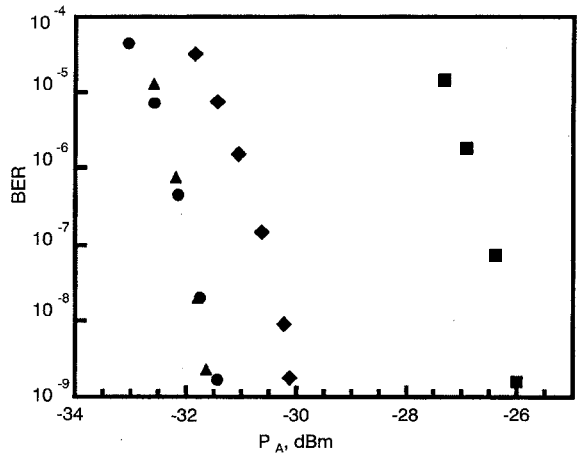

Fig. 4 *BER against P_A for three different levels of OBI*

$MI_S = MI_C$ = 180%
● RIN_{OBI} = –90.9dB/Hz, P_B = –19dBm
◆ RIN_{OBI} = –81.5dB/Hz, P_B = –16dBm
■ RIN_{OBI} = –77.7dB/Hz, P_B = –13dBm
▲ No OBI

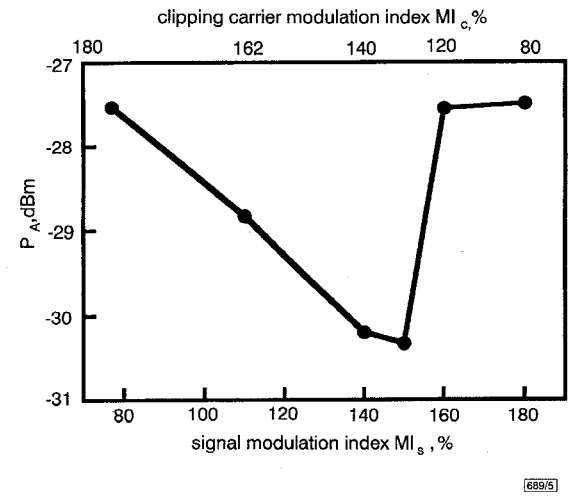

Fig. 5 *Minimum required received power from laser A for different combinations of clipping carrier and CDMA signal when total driving power was fixed*

Fig. 4 shows the measured results when $MI_S = MI_C$ = 180%, for the cases of no OBI and OBI levels given by RIN_{OBI} = –90.9, –81.5 and –77.7dB/Hz, respectively. Here, RIN_{OBI} is defined as $\langle i_{OBI}^2 \rangle / I_A^2$ where i_{OBI}^2 is the spectral density of the OBI noise current and I_A is the received photocurrent from laser A. It is interesting to note that there was a negligible system power penalty even when the OBI level was as high as –90.9dB/Hz. In addition, if we consider the system dynamic range (DR) as the ratio of maximum to minimum allowable received optical power [4], it is given by (P_B – 3) – P_A [dB] and is ~10dB for RIN_{OBI} = –81.5 or –77.7dB/Hz. This is much higher than the 2.5dB DR obtained previously when the

clipping carrier was absent [1]. Consequently, the power control requirement on S-CDMA technique can be relaxed significantly.

Although the added coherent clipping carrier provides an excellent OBI suppression capability and a large system DR, it consumes a significant amount of RF driving power to laser A. Conversely, it is conjectured that the clipping carrier can suppress OBI more effectively than the S-CDMA signal. It is therefore important to find a balance between the driving power levels of the clipping carrier and the S-CDMA signal. Fig. 5 shows the results of P_A against different values of MI_S and MI_C when the total driving power was fixed. We can see that there indeed exists an optimum (coherent) combination of the clipping carrier and the S-CDMA signal power, i.e. a minimum P_A of –30.5dBm was obtained when MI_S = 150% and MI_C = 130%. Also, when most of the driving power is allocated to either the clipping carrier or the S-CDMA signal, the resultant power levels of P_A were increased by 3dB compared to the optimum case.

Conclusion: In this Letter, we have experimentally demonstrated that an in-band clipping carrier, when coherently combined with a Walsh-code-based S-CDMA signal, can effectively suppress OBI in a PON or WDMA network. When the total driving power was fixed, we found that an optimum combination ratio of the two signals exists to achieve a maximum system power budget. Our experimental results showed that, under the condition of no bandwidth wasted on the in-band clipping carrier, a negligible system power penalty can be achieved even when the OBI-induced intensity noise was as high as –90.9dB/Hz. In addition, a large system dynamic range of 10dB can be obtained to relax the tight power control requirement on S-CDMA signals.

23 July 1997
Electronics Letters Online No: 19971275

B.H. Wang, C.C. Hsiao and W.I. Way (*Department of Communication Engineering, National Chiao-Tung University, Hsin-Chu, Taiwan, Republic of China*)

E-mail: wiway@cc.nctu.edu.tw

References

1 HSIAO, C.C., WANG, B.H., and WAY, W.I.: 'Multiple access in the presence of optical-beat and co-channel interference using Walsh-code-based synchronised CDMA technique', *IEEE Photonics Technol. Lett.*, 1997, **8**, pp. 1173–1175

2 WOODWARD, S.L., LU, X., DARCIE, T.E., and BODEEP, G.E.: 'Reduction of optical-beat interference in subcarrier networks', *IEEE Photonics Technol. Lett.*, 1996, **8**, pp. 694–696

3 SASAI, H., YAMAMOTO, H., UTSUMI, K., and FUJITO, K.: 'Optical access links suppressing optical beat interference with FP-LDs for microwave transmission'. Int. Topical Meeting on Microwave Photonics, Tech. Dig., 1996, pp. 237–240

4 FELDMAN, R.D., WOOD, T.H., RAYBON, G., and AUSTIN, R.F.: 'Effect of optical beat interference on the dynamic range of a subcarrier multiple access passive optical network using Fabry-Perot laser', *J. Lightwave Technol.*, 1996, **5**, pp. 711–715

5 WOOD, T.H., and SHANKARANARAYANAN, N.K.: 'Operation of a passive optical network with subcarrier multiplexing in the presence of optical beat interference', *J. Lightwave Technol.*, 1993, **10**, pp. 1632–1640

Time-space-conversion optical signal processing using arrayed-waveguide grating

T. Kurokawa, H. Tsuda, K. Okamoto, K. Naganuma, H. Takenouchi, Y. Inoue and M. Ishii

Indexing terms: Optical communication equipment, Gratings in fibres

The authors propose time-space-conversion optical signal processing using an arrayed-waveguide grating. It provides a wide time window, compatibility with fibre optics, compactness, and integration capabilities. Pulse train generation is demonstrated to confirm its performance at the wavelength of 1.55μm.

Optical signal processing based on time-space-conversion is highly attractive, especially for ultrafast signal processing applications in high-speed optical communcation systems with a data rate of more than 100 Gbit/s. Such processing enables many operations such as the formation, reshaping, pattern recognition and even routing of an ultrafast bit stream, which are difficult to do by traditional electronic means. This technology has been widely demonstrated in the wavelength range of 0.4–0.85μm by using free-space optics with diffraction grating pairs and lenses [1 – 4]. In such a grating system, however, the time window is determined by the size of the diffraction grating and spatial filter, and it is difficult to make it compact.

In this Letter, we propose time-space-conversion optical signal processing using an arrayed-waveguide grating (AWG) and demonstrate pulse train generation at the communication wavelength of 1.55μm.

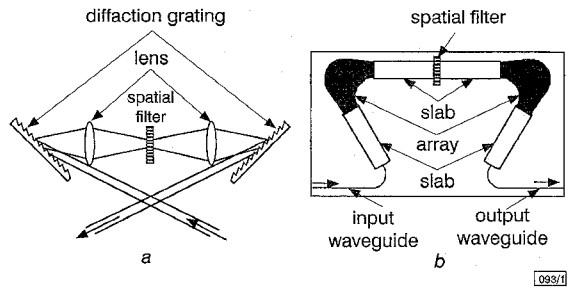

Fig. 1 *Schematic diagram of time-space-conversion processing system using diffraction gratings (DGs), and arrayed-waveguide gratings (AWGs)*

a DGs
b AWGs

Fig. 1 shows a schematic diagram of time-space-conversion processing systems using *a* diffraction gratings (DGs) and *b* arrayed-waveguide gratings (AWGs). In both systems, a temporal waveform carries spatial information on the dispersive element and is converted to a temporal frequency spectrum in the focal plane. The frequency spectrum is then modulated in parallel by a spatial filter and reconverted to a reshaped temporal waveform. When the waveform $u(t)$ is incident on the dispersive elements, such as a DG and an AWG, with the incident angle so as to produce the surface normal diffracted beam with the carrier lightwave frequency ν_0, it is transformed into $u(t - n/\beta x/c)$ on the x axis lying along the exit surface of the dispersive element, where β is a dispersion parameter, c is the speed of light, and n is the refractive index of the media through which the light propagates. The dispersion parameter is given as

$$\beta = \nu_0 \frac{d\theta}{d\nu} = \frac{mc\nu_0}{nd\nu^2} \quad (1)$$

where m is the diffraction order and d is the periodical pitch of the dispersive elements. The maximum time window T_0 is determined by $n\beta x/c$, hence:

$$T_0 = \frac{n\beta}{c} Nd = \frac{mN}{\nu_0} \quad (2)$$

where N is the number of illuminated lines of the DG or waveguides of the AWG. The diffraction order of the DG is limited to a small value, typically m = 1, as it is proportional to the grating pitch, whereas AWGs usually have a large diffraction order (30–200) as it is proportional to the path length difference between neighbouring waveguides [5]. This means we have some design flexibility in that the dispersion parameter value can be made quite large for an arbitraray diffraction order in the AWG system, and this results in a long total time window even if N is limited to a smaller value than that in the DG system.

Conversely, in the DG system pulsewidth τ in the pulse trains is usually limited by the spatial filter size, H, as follows:

$$\tau \geq \frac{cf}{nd\nu_0^2 H} \quad (3)$$

where f is a focal length of a lens. The pulsewidth in the AWG system, however, is determined only by the diffraction order such that

$$\tau \geq \frac{m}{\nu_0} \quad (4)$$